

Zeeman deceleration of H and D

S. D. Hogan, D. Sprecher, M. Andrist, N. Vanhaecke,* and F. Merkt
Laboratorium für Physikalische Chemie, ETH Zürich, CH-8093, Switzerland
 (Received 22 June 2007; published 17 August 2007)

Hydrogen and deuterium atoms in supersonic jet expansions have been decelerated using a multistage Zeeman decelerator. The properties of the decelerator have been completely characterized in a series of experiments in which (i) the initial longitudinal velocities of the decelerated atoms, (ii) the maximum magnetic field strength, and (iii) the duration of zero-field intervals between successive field pulses in neighboring deceleration stages were systematically varied. Experiments using Ar and Kr as carrier gases have clearly revealed that the H atoms are located at the surface of the jet expansion cone in each case. Comparison of the results of these experiments with numerical simulations of the atom trajectories through the decelerator provides a full description of the phase-space distribution of the decelerated atoms. Evidence is presented of transverse guiding of the beam and of a partial redistribution of the H atom population among the M_F components of the $F=1$ manifold at times when the magnetic field strength approaches zero.

DOI: 10.1103/PhysRevA.76.023412

PACS number(s): 32.60.+i, 33.80.Rv

I. INTRODUCTION

In recent years efforts have been invested in the development of quantum-state-selective techniques to manipulate the translational motion of atoms and molecules in pulsed supersonic beams. This development has been motivated by the prospects of performing high-resolution spectroscopy in the gas phase [1] and of studying atomic and molecular collisions either at low temperatures or with a high degree of control over the kinetic energies of the colliding particles [2]. Initially, emphasis was placed on exploiting the forces exerted by electric field gradients upon atoms and molecules exhibiting permanent electric dipole moments (i.e., atoms and molecules in states with a linear Stark effect) which led to the development of the techniques of multistage Stark deceleration [3,4] and Rydberg Stark deceleration [5–7]. Whereas multistage Stark deceleration is suitable for ground state polar molecules, Rydberg Stark deceleration is in principle applicable to all atoms and molecules, but these must first be excited to Rydberg states and care must be taken to ensure that these states have sufficiently long lifetimes for efficient deceleration. Each of these deceleration techniques is quantum-state selective, the quantum-state selectivity arising from the facts that (i) the electric field gradients employed can be tailored to decelerate only those particles in states with a particular Stark shift and (ii) they rely on pulsed supersonic expansions in which the temperatures associated with internal (electronic, vibrational, and rotational) motion can be sufficiently low that only the ground state is appreciably populated.

With the desire to extend the range of ground state species which may be decelerated and manipulated to include all atoms and molecules with a linear electron Zeeman effect, we have recently constructed a multistage Zeeman decelerator [8], the magnetic analog of the multistage Stark decelerator [3]. This instrument is suitable for the deceleration of

particles with unpaired electrons and is therefore of particular interest for studies of the spectroscopic and chemical properties of radicals at low temperature [9].

The use of magnetic field gradients to manipulate atomic and molecular beams dates back to the work of Gerlach and Stern in the 1920s [10–12]. By propagating a beam of silver atoms through an inhomogeneous magnetic field, they were able to observe a transverse separation of the beam and thus demonstrated space quantization. Their experiment relied on the force \vec{F} exerted on a particle with an effective magnetic moment $\vec{\mu}_{\text{eff}}$ by an inhomogeneous magnetic field \vec{B} , such that

$$\vec{F} = -\nabla(\vec{\mu}_{\text{eff}} \cdot \vec{B}).$$

The deflection of molecular beams in inhomogeneous magnetic fields has also played a role in the early development of nuclear magnetic resonance spectroscopy [13]. However, the only experiment that we are aware of in which a magnetic field gradient has been used to apply a force along the axis of propagation of a molecular beam involved the generation of turbulence in a continuous stream of gaseous O₂ [14]. In this experiment, the gradient associated with a single dc electromagnet was exploited for studies of gas dynamics.

In a recent proof-of-principle experiment, we have developed and tested a six-stage Zeeman decelerator to slow down H atoms seeded in a pulsed supersonic beam of xenon from an initial longitudinal velocity of 313 m/s to a final velocity of 225 m/s [8]. The sequence of pulsed currents applied to each of the six solenoids of which this device was composed was calculated so as to remove a constant longitudinal kinetic energy from the beam of H atoms at each stage. The principles of phase stability used in charged particle accelerators [15,16] were employed to keep the decelerated bunch of H atoms together both longitudinally and transversely as they propagated through the device. This first prototype was operated at a pulsed current of 140 A, resulting in a maximum magnetic field strength of 0.8 T on axis at the center of each solenoid. Moreover, the solenoids could not be pulsed independently because of constraints imposed by the design

*Current address: Laboratoire Aimé Cotton, CNRS II, Bâtiment 505, Campus d'Orsay, 91405 Orsay cedex, France

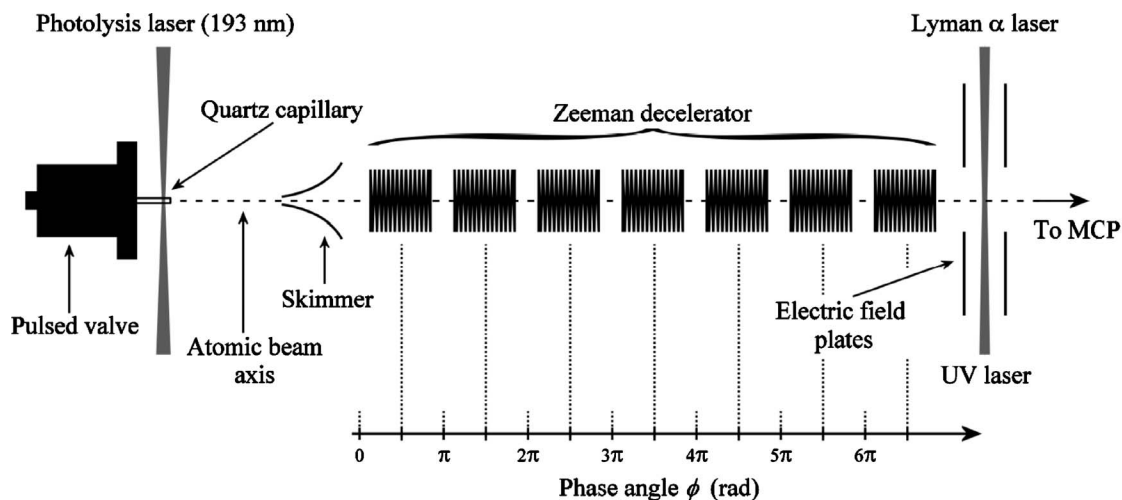


FIG. 1. Schematic diagram of the experimental setup (not to scale). The H (D) atomic beam is prepared in a pulsed supersonic expansion by 193 nm photolysis of NH_3 or ND_3 , respectively. After propagating through a 2 mm diameter skimmer, the beam enters the Zeeman decelerator. The TOF from the point of production of the H (D) atoms to the end of the decelerator is measured by two photon excitation to Rydberg states followed by pulsed electric field ionization. The resulting ions are then detected on a microchannel plate (MCP) detector (not pictured). The phase angle ϕ with respect to the first solenoid of the decelerator is indicated in the lower part of the figure (see text for details).

of the electronics but had to be operated as two sets of three solenoids connected in series. The latter restriction led to an undesired period of zero magnetic field between the application of pulses to neighboring solenoids. The resulting blurring of the time-of-flight (TOF) profiles was tentatively interpreted as arising from a redistribution of population among the magnetic sublevels of the ground state of the H atom. More recently, Narevicius and co-workers have proposed Zeeman deceleration as a means to slow paramagnetic atoms or molecules on the basis of simulations only [17].

The present article describes a second generation of Zeeman decelerator consisting of seven stages for which the limitations described above have been alleviated: Currents of up to 250 A can now be applied to each solenoid in this device without affecting the temporal characteristics of the pulses and each solenoid can be pulsed independently. These improvements have permitted the exploration of a wider range of experimental conditions than previously possible. In particular they have made it possible to carry out (i) experiments with both H and D atoms, (ii) tests with carrier gases other than xenon (i.e., argon and krypton), (iii) studies to quantify the role of zero-field periods between pulses applied to successive solenoids, and (iv) deceleration of atoms with a much wider range of initial velocities. A more detailed understanding of multistage Zeeman deceleration has resulted from these measurements and the purpose of this article is to provide a quantitative analysis of these new results.

II. EXPERIMENT

The Zeeman deceleration experiments reported here were performed on ground state atomic hydrogen and deuterium formed by 193 nm photolysis of NH_3 or ND_3 in a seeded supersonic expansion using the radical source described in Ref. [18]. A schematic diagram of the experimental setup is

presented in Fig. 1. The ammonia is photolyzed by focusing the output beam of an ArF excimer laser in a 10 mm long quartz capillary (1 mm inner diameter) mounted on the base plate of a pulsed valve. Efficient cooling of the seeded beam of H (D) atoms is achieved during the adiabatic expansion which occurs upon the exit of the gas pulse from the capillary. The resulting longitudinal temperature of the H atoms (extracted from the longitudinal velocity distribution) when operating the pulsed valve at an absolute stagnation pressure of 4 bar and using a 10:1 Ar: NH_3 mixture is ~ 2 K. Approximately 20 mm after exiting the quartz capillary, the atomic beam is collimated by a 2 mm diameter skimmer before it enters the first solenoid of the decelerator, positioned 75 mm from the tip of the skimmer.

The solenoids used in our seven-stage decelerator have an inner diameter of 5 mm and are 7.8 mm long. They are composed of 42 windings of 300 μm copper wire wound in two layers of 21 windings each. The spacing between each solenoid on the axis of the decelerator is 3.2 mm and thus the decelerator has a spatial period on axis of 11 mm. Using custom-made electronics, built in house, to drive pulsed currents of up to 250 A through the solenoids for durations of several tens of microseconds, rise and fall times of the magnetic field in each solenoid of ~ 5 and ~ 4 μs , respectively, are obtained. These characteristics have been measured using both a small pick-up solenoid positioned on axis at the center of each solenoid and by observing the returning current from each solenoid as a potential drop across a 10 m Ω shunt resistor. A typical measurement of the magnetic field made using the pick-up solenoid is displayed in Fig. 2(a). For a current of 250 A the strength of the magnetic field on axis at the center of each solenoid amounts to ~ 1.4 T. In order to remove the thermal energy dissipated during operation of the decelerator, the solenoids are mounted in a water-cooled ceramic block.

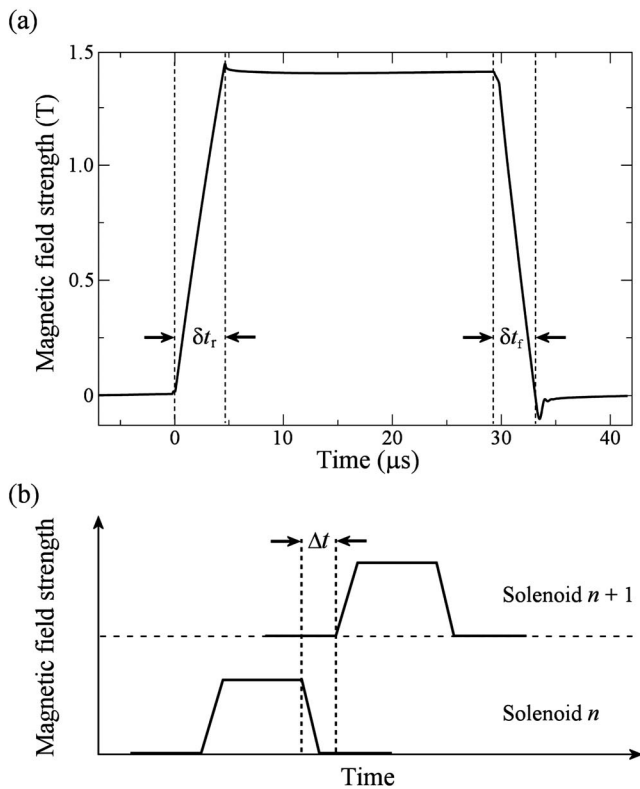


FIG. 2. (a) Measurement of the temporal profile of the magnetic field on axis at the center of one of the decelerator solenoids made via integration of the electrical potential generated in a small pick-up solenoid. For this particular solenoid, the rise time δt_r and fall time δt_f amount to 4.7 and 3.9 μs , respectively. (b) Schematic timing diagram indicating the definition of the time delay Δt between the initiation of the switch-off and switch-on of the magnetic field in adjacent solenoids (labeled n and $n+1$) in the decelerator.

In the absence of the field, the hyperfine interaction gives rise to a splitting of the 1^2S ground state of H into $F=0$ and $F=1$ states, where F is the total spin quantum number [see Fig. 3(a)]. Upon the application of a magnetic field, the $F=0$ state is shifted to lower energy whereas the $F=1$ state is split into a manifold of three M_F states. The $M_F=0$ and $+1$ states are shifted to higher energies by the magnetic field while the $M_F=-1$ state is shifted to lower energies. At high magnetic field strengths the states can be classified according to their value of m_s , which amounts to $+\frac{1}{2}$ ($-\frac{1}{2}$) for the two states that are shifted upwards (downwards). Figure 3(b) displays the magnetic field distribution in one solenoid through which a current of 250 A flows. An important feature of this distribution is the concave nature of the radial profile in the high-field region inside the solenoid. This curvature naturally guides atoms in the low-field seeking $F=1$, $M_F=0$, $+1$ levels and ensures transverse stability of the deceleration process.

Prior to switching on the first solenoid of the Zeeman decelerator, the H atoms in the supersonic beam are distributed statistically among the $F=0$ and the three $F=1$ states. When the magnetic field is switched on, the atoms in the $F=1$ state populate each of the three corresponding M_F states with equal probabilities. The manner in which the decelerator is operated involves acting on the atoms in the up-

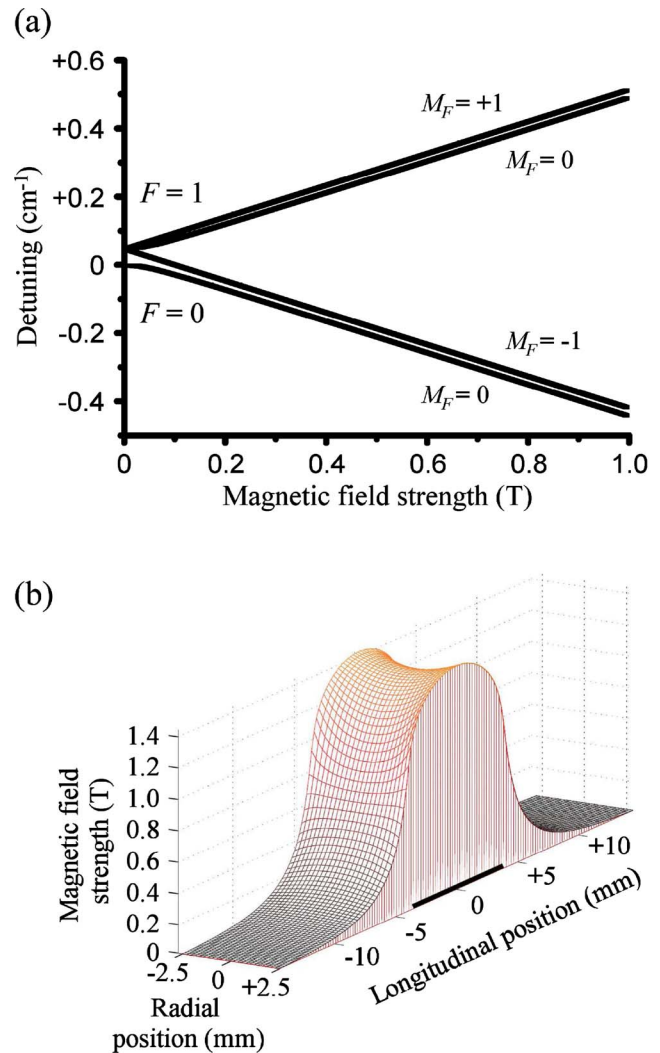


FIG. 3. (Color online) (a) The Zeeman effect in the 1^2S ground state of atomic hydrogen. The hyperfine interaction splits the ground state into $F=0$ and $F=1$ states, where F is the total spin quantum number. Upon application of the magnetic field, the $F=1$ state splits into a manifold of three M_F states, two of which are shifted to higher energies and one to lower energy as the field strength increases. (b) Map of the longitudinal and radial magnetic field distribution in each solenoid of the Zeeman decelerator calculated for an operating current of 250 A. The position and spatial extension of the solenoid is indicated by the thick black line on the axis representing the longitudinal position.

per $M_F=0$ and $M_F=+1$ states which lose kinetic energy as they travel into a magnetic field of increasing strength to compensate for the increase in internal Zeeman energy. The current in each solenoid is switched off before the decelerated atoms are subject to the negative magnetic field gradient associated with the end of the solenoid, to prevent them from regaining the kinetic energy lost when entering. The switching on and off processes are repeated at each solenoid in the series. The delay Δt between the switch-off time of solenoid n and the switch-on time of solenoid $n+1$, as illustrated in Fig. 2(b), can be freely adjusted.

The computer-controlled deceleration pulse sequences applied to the solenoids of the decelerator are calculated using the principles of phase stability originally employed in charged particle accelerators and now also used in the operation of multistage Stark decelerators [19,20]. These pulse sequences are calculated for a bunch of particles with an initial longitudinal velocity distribution centered around a chosen mean value. The representative particle of this bunch which has an initial longitudinal velocity equal to the mean of the distribution and traverses the decelerator on axis is termed the “synchronous particle.” For a given operating current and initial longitudinal velocity of the synchronous particle, a phase angle ϕ is chosen within the longitudinal periodic structure of the decelerator at which the current is switched off in each solenoid. A phase angle of 0° corresponds to switching off the current in the solenoids when the synchronous particle is located at the midpoint between two successive solenoids, while a phase angle of 90° corresponds to switching off the current when the synchronous particle has reached the center of the solenoids (see Fig. 1). Strictly, the definition of a phase angle requires fall times of the magnetic field in each solenoid which are negligible compared to the time scale of the translational motion of the bunch of decelerated atoms. Consequently the phase-angle concept as used in this article refers to the time at which the switch off of the current in each solenoid is initiated. As was first shown for charged particle accelerators [15,16], the velocity range of particles which traverse the decelerator in a stable way decreases rapidly as the phase angle approaches 90° . A compromise must therefore be made between the maximal longitudinal kinetic energy removed from the synchronous particle per stage and the acceptance of the decelerator in phase space. As the decelerator used in the experiments reported here is composed of only seven stages, the effects arising from non-phase-stable traversal of the instrument, though noticeable, are not as significant as would be the case in a longer device.

The timing of the experiment is illustrated in Fig. 4. A measurement cycle begins at t_{exc} when the H atoms are produced by excimer laser photolysis. The solenoids in the decelerator are then successively switched on and off at times precalculated for a given velocity class. Because the switch-on time of the first solenoid is not relevant provided that the field is on when the atoms approach the decelerator, the relative switch-on and -off times are defined with respect to the switch-off time of the first solenoid [t_0 in Fig. 4(a)]. In Fig. 4(b), a pulse sequence is presented which is calculated to decelerate H atoms assuming an initial longitudinal velocity of the synchronous atom of 527 m/s, a current of 250 A, and a phase angle of 55° . The durations of the pulses applied to successive solenoids in this sequence increase as the atoms decelerate. This is made explicit in panel (c) where the duration of each pulse is plotted against the time at which it is turned on.

The H (D) atoms which arrive at the end of the decelerator are detected by pulsed electric field ionization following a two-photon excitation via the 2^2P state to ns and nd Rydberg states around $n=30$ between a pair of metallic plates as depicted in Fig. 1. The detection time is therefore given by the timing of the laser pulses involved in this process. What

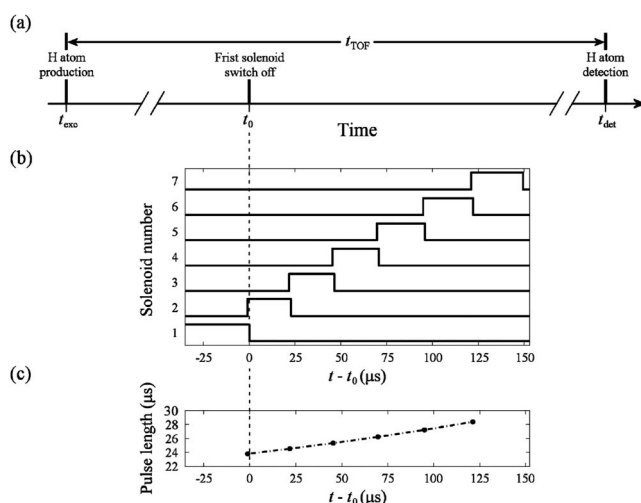


FIG. 4. (a) General timing scheme for the operation of the Zeeman decelerator. The H atoms are produced at time t_{exc} with the first solenoid of the decelerator then switched off at time t_0 such that the synchronous atom enters the decelerator at a predefined phase angle. The two-photon excitation and field ionization take place at a time t_{det} such that the TOF is given by $t_{\text{det}} - t_{\text{exc}}$. (b) A typical computer controlled pulse sequence calculated to decelerate a bunch of H atoms with a mean initial longitudinal velocity of 527 m/s to a final velocity of 415 m/s over seven decelerator stages switched at a 55° phase angle and operated at a current of 250 A. The temporal overlap Δt between consecutive pulses in this sequence is $-1 \mu\text{s}$ (see Fig. 2). As the atoms lose longitudinal kinetic energy, the pulses become longer as can be seen in (c) where the duration of the pulses applied to each of the solenoids is plotted against the time at which each is switched on.

we shall refer to as the TOF of the H atoms through the decelerator corresponds to the difference between this detection time and the time at which the H atoms are produced [t_{exc} , see Fig. 4(a)]. The vuv radiation at Lyman α required to drive the transition from the 1^2S ground state of atomic hydrogen to the 2^2P state is generated by resonance-enhanced difference-frequency mixing of laser radiation generated by two Nd:YAG-pumped pulsed dye lasers. This four-wave mixing is carried out in a cell filled with ~ 10 mbar krypton. The frequency-doubled output of a third Nd:YAG-pumped pulsed dye laser is then used to drive the second step in the two-photon transition. The excited Rydberg atoms are ionized using a pulsed electric field of 1.8 kV/cm and the resulting ions are accelerated toward a microchannel plate detector. The TOF profile of the H atoms is obtained by scanning the time at which the uv and vuv laser beams cross the beam of H atoms with respect to the excimer laser pulse used to generate the H atoms.

III. SIMULATION

To assist in the analysis of the experimental data, Monte Carlo particle trajectory simulations have been performed under the conditions for which each set of experiments was carried out. In these calculations an ensemble of atoms is generated with phase-space properties matching those deter-

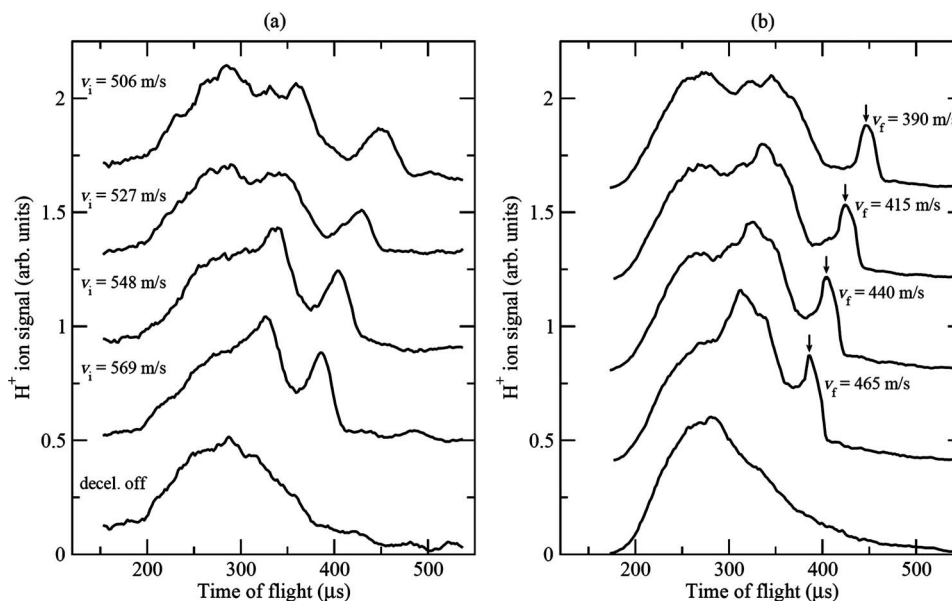


FIG. 5. TOF profiles demonstrating the deceleration of H atoms using pulse sequences calculated for synchronous atoms with initial longitudinal velocities of 569, 548, 527, and 506 m/s when the decelerator was operated at a current of 250 A and a phase angle of 55° . (a) Experimental TOF profiles, (b) simulated TOF profiles. The final velocities of the decelerated atoms determined from the simulations are indicated alongside the vertical arrows in panel (b). The bottom profile in each panel represents the TOF of the H atoms with the decelerator off. For clarity of presentation the upper profiles in each panel are vertically offset.

mined experimentally for the pulsed atomic beam in free flight. Initially, the H atoms are distributed equally among the four M_F sublevels of the 1^2S state. All particle trajectories are then calculated from the known three-dimensional magnetic field distribution [21], and the same pulse sequences, including the finite rise ($5 \mu\text{s}$) and fall ($4 \mu\text{s}$) times of the magnetic field in each solenoid, as those employed in the experiments. Effects of collisions between the atoms in the gas pulse are not included. Because the experimental parameters have all been measured independently the simulations do not involve any adjustable parameters.

An important aspect of the particle trajectory simulations is the set of initial transverse phase-space properties of the atomic beam. Because the mass ratio $m_{\text{CG}}:m_{\text{H}}$ between the carrier gas (CG=Ar or Kr) and the seed gas (H) is large, the H atoms tend to be located at the surface of the gas expansion cone and possess a significant transverse velocity. This effect was clearly visible in our imaging experiments on H Rydberg atoms (see Fig. 2 of Ref. [22]). A radial velocity, from a distribution with a mean of 24 m/s and standard deviation of 12 m/s (extracted from Rydberg atom imaging data), was attributed to each atom to account for the velocity distribution in the transverse dimension.

At times when the magnetic field strength experienced by the H atoms along their trajectory approaches zero, a redistribution of the population among M_F states can occur as a result of Majorana transitions [23] or of transitions driven by rf noise in the solenoids. The transitions occur primarily among the M_F components of the $F=1$ state. To take these transitions into account in the simulations and to quantify their effect upon the deceleration process, the population can be redistributed among these states each time the current in a solenoid is switched off. The transitions are assumed to take

place with an equal probability of $p/2$ to each of the other two M_F sublevels, where p represents the probability that a given atom undergoes a change of M_F .

IV. RESULTS AND DISCUSSION

A. Deceleration of H atoms seeded in an Ar beam

The maximum current at which the Zeeman decelerator can currently be operated is 250 A. This corresponds to a maximal magnetic field strength on axis in each solenoid of 1.4 T. In Fig. 5(a) a set of measurements is displayed in which the initial longitudinal velocity of the synchronous atom was varied by adjusting the temporal pulse sequence applied to the decelerator. The solenoids were operated at the maximal current and switched at a constant phase angle of 55° for the synchronous atom. The bottom profile in this figure corresponds to the H atom TOF profile obtained when the decelerator was off and contains information on the velocity distribution of the H atoms in the beam. The other profiles correspond to deceleration measurements recorded for pulse sequences calculated for the deceleration of synchronous atoms with initial velocities of 569, 548, 527, and 506 m/s as indicated.

Comparison of the TOF profiles in Fig. 5(a) reveals that (i) the total number of H atoms detected is larger when the decelerator is turned on than when it is turned off because of the transverse guiding properties of the magnetic field distribution [see Fig. 3(b)], (ii) a bunch of H atoms is strongly decelerated and forms an isolated late peak in the TOF profile that shifts to even later times as the initial velocity is reduced, and (iii) an additional maximum in the TOF profile appears at $\sim 330 \mu\text{s}$ when the initial longitudinal velocity of

the synchronous atom is 569 m/s and shifts a little toward later times in the upper profiles. These experimental profiles are reproduced almost quantitatively in the simulations of the trajectories of the atoms through the decelerator presented in Fig. 5(b). The small differences between the widths of the bunches of decelerated atoms in the experiment and the simulations are likely to arise from the uncertainties in the exact position and size of the volume determined by the intersection of the two laser beams used to detect the atoms at the end of the decelerator (see Fig. 1).

It is not possible to extract the final longitudinal velocities of the decelerated atoms directly from the experimental data, but only by comparison with the particle trajectory simulations. For each of the initial longitudinal velocities listed in Fig. 5(a) the final velocities are calculated to be 465, 440, 415, and 390 m/s, respectively, as indicated by the positions of the vertical arrows in Fig. 5(b). From the difference between each of these final velocities and the initial velocities of the synchronous atoms, we calculate the mean loss of kinetic energy when operating the decelerator at 250 A and a phase angle of 55° to be 0.55 meV ($\equiv 4.4 \text{ cm}^{-1}$) or 0.079 meV ($\equiv 0.63 \text{ cm}^{-1}$) per stage. The simulations can also be used to analyze the evolution of the phase-space distribution during the deceleration process, as is illustrated in Fig. 6 for the deceleration of the H atoms with an initial longitudinal velocity of 506 m/s.

The upper panel, Fig. 6(a), represents the calculated H atom signal as a function of longitudinal velocity and TOF through the decelerator. The data presented in this panel were calculated for a maximal current of 250 A and a 55° phase angle. The intensity scale is indicated by the inset color bar. The full profile in the lower panel (b) represents the TOF distribution under these conditions whereas the dashed profile represents the TOF distribution when the decelerator is off. The maximum of this velocity distribution lies at 750 m/s. A comparison between the solid curve and the data in panel (a) provides the explanation for the structures observed in the TOF profile. Three regions, labeled A, B, and C in Fig. 6(a), are discussed in more detail below.

In the first region A the H atom signal corresponds to the maximum of the velocity distribution in the beam. These atoms have longitudinal velocities ≥ 506 m/s and are therefore not significantly affected by the operation of the decelerator. The TOF distribution shows the expected behavior, namely, that the fast atoms have the shortest TOF. The region labeled C demonstrates that the decelerated atoms are those in the $F=1, M_F=0, +1$ magnetic sublevels for which the deceleration pulse sequence was calculated. The corresponding late TOF peak in the lower panel is seen to be composed primarily of atoms moving with a velocity of ~ 390 m/s with a small contribution from atoms with velocities between 390 and 450 m/s. The presence of this intense bunch of slow atoms is indicative of the phase-stable operation of the decelerator. The middle region B corresponds to an enhancement of the H atom signal at a TOF of $\sim 340 \mu\text{s}$. This signal can be attributed to those atoms in the $F=1, M_F=0, +1$ states which enter the decelerator with a velocity slightly greater than that of the synchronous atom. These atoms travel further into each of the solenoids than the synchronous atom while the field is on and are subject to longitudinal

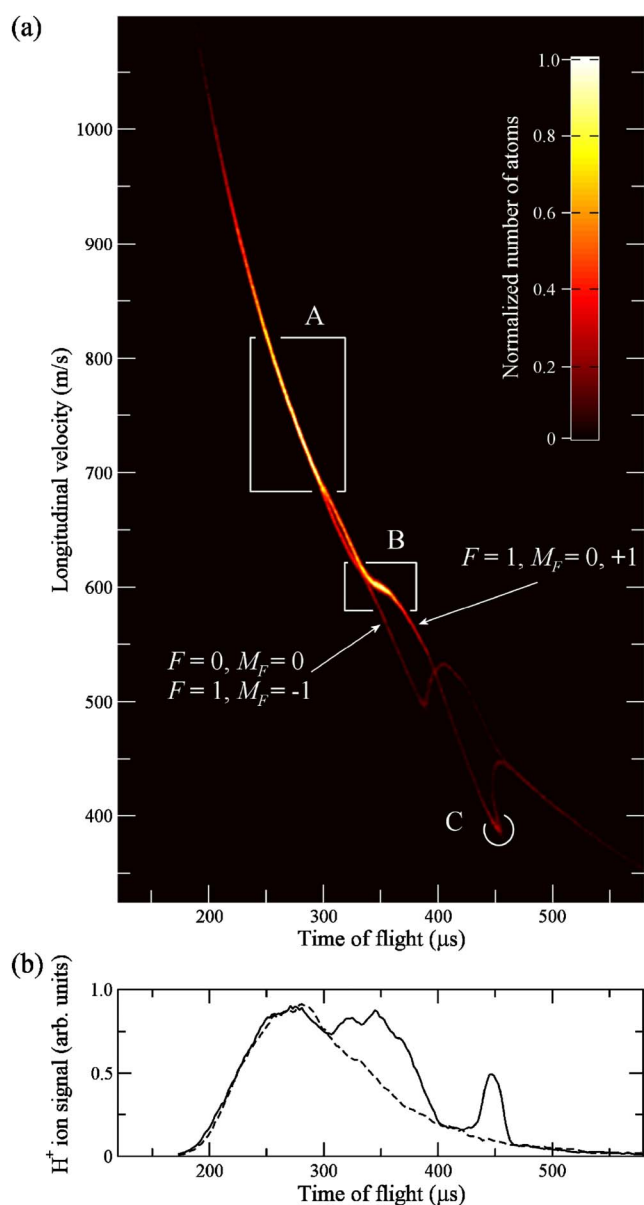


FIG. 6. (Color online) Simulated characteristics of the beam of H atoms. (a) Color map indicating the H atom signal as a function of longitudinal velocity and TOF. The decelerator is assumed to operate at 250 A with a pulse sequence calculated to decelerate a synchronous atom with an initial longitudinal velocity of 506 m/s to a velocity of 390 m/s at a 55° phase angle. The color gradient indicates the number of atoms with a particular longitudinal velocity. The feature enclosed by box A corresponds to the bunch of atoms unaffected by the operation of the decelerator, that in box B arises as a result of the combination of longitudinal bunching and transverse guiding in the decelerator, and that labeled C represents the bunch of decelerated atoms. The TOF profile corresponding to this velocity distribution is represented in (b) by the solid curve, while the dashed curve represents the simulated TOF profile with the decelerator off.

bunching and strong transverse guiding, giving rise to a locally enhanced signal. These effects are particularly noticeable in these experiments because of the short length of the decelerator. The trajectories of the corresponding atoms are

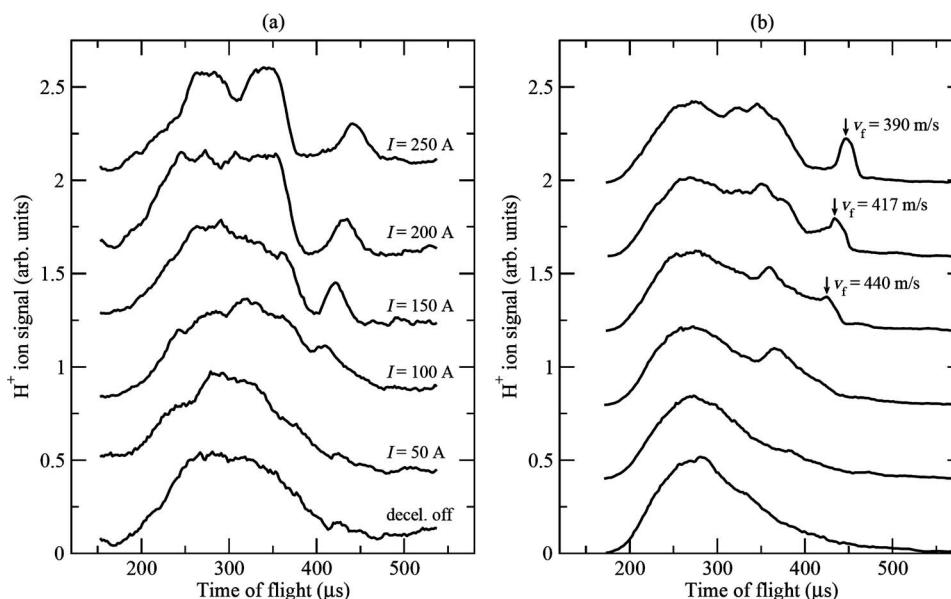


FIG. 7. TOF profiles demonstrating the deceleration of H atoms at different decelerator operating currents. The deceleration pulse sequence was calculated for a synchronous atom with an initial longitudinal velocity of 506 m/s and for a phase angle of 55° . The current at which the decelerator was operated was varied from 50 to 250 A (corresponding to a maximum magnetic field strength on axis in each solenoid of 0.3 and 1.4 T, respectively). (a) Experimental TOF profiles, (b) simulated TOF profiles. The final velocities of the decelerated atoms determined from the simulations are indicated alongside the vertical arrows in panel (b). The bottom profile in each panel represents the TOF of the H atoms with the decelerator off. For clarity of presentation the upper profiles in each panel are vertically offset.

not phase stable and the longitudinal velocities disperse as the atoms propagate through the decelerator; i.e., the faster atoms are always accelerated more than the slower ones. In a longer decelerator, this longitudinal dispersion would eventually lead to the disappearance of this structure in the TOF profile.

Presented in Fig. 7 are the results of a set of experiments in which the operation of the Zeeman decelerator was studied as a function of the pulsed current applied to each solenoid. For each of the profiles in this figure, the deceleration pulse sequences were calculated for synchronous atoms with a fixed initial longitudinal velocity of 506 m/s. As expected, the TOF of the decelerated bunch of atoms increases as the amplitude of the pulsed current is increased from 50 to 250 A, corresponding to a maximum magnetic field strength on axis in each solenoid of 0.3 and 1.4 T, respectively. The decelerated bunch of atoms only forms a distinct peak in the TOF profile for currents larger than 150 A.

The results of the corresponding particle trajectory simulations are presented in Fig. 7(b). The final velocities of the decelerated atoms at operating currents of 150, 200, and 250 A can be determined from the simulations to be 440, 417, and 390 m/s, respectively, and the corresponding losses of longitudinal kinetic energy amount to 0.33 meV ($\equiv 2.6 \text{ cm}^{-1}$), 0.43 meV ($\equiv 3.5 \text{ cm}^{-1}$), and 0.54 meV ($\equiv 4.4 \text{ cm}^{-1}$). These changes in kinetic energy are in good agreement with those obtained from the data presented in Fig. 5 and exhibit the expected linear variation as a function of the operating current. We attribute the small differences in the experimental TOF profiles of the undecelerated part of the gas pulse between the top profile of Fig. 5(a) and that of Fig. 7(a), which were recorded using the same pulse se-

quences and pulsed currents, to differences in the alignment of the laser beams at the detection point. This alignment does not affect the TOF of the decelerated bunch of atoms, nor does it significantly affect its profile. The three-dimensional particle trajectory simulations therefore capture the main characteristics of the deceleration process and demonstrate that (i) the pulse sequences that are generated prior to running the experiment are close to optimal and (ii) the simulations provide an accurate description of the deceleration process over a wide range of operating currents.

B. M_F -changing transitions at near-zero magnetic field

In the experiments carried out with our previous Zeeman decelerator [8] the TOF profiles observed did not exhibit structures as sharp as predicted by simulations in which redistribution of the population of the $F=1$ states was disregarded. This blurring was attributed to transitions from the $F=1$, $M_F=0$, and $+1$ states, for which the deceleration pulse sequence was calculated, to the $M_F=-1$ state of the same F manifold at times when the atoms experienced a near-zero magnetic field. Indeed, technical limitations of the high current pulse generators used in that work imposed a delay of at least 100 ns between the end of the fall of the current in each solenoid in the decelerator and the switch-on time of the next solenoid. This gave rise to short periods of time during which the magnetic field experienced by the atoms was sufficiently close to zero for M_F -changing transitions to occur.

With the new high current pulse generators, the origin of these M_F changes has been investigated in more detail by varying the time separation between the pulses of current applied to adjacent solenoids. The results of this investiga-

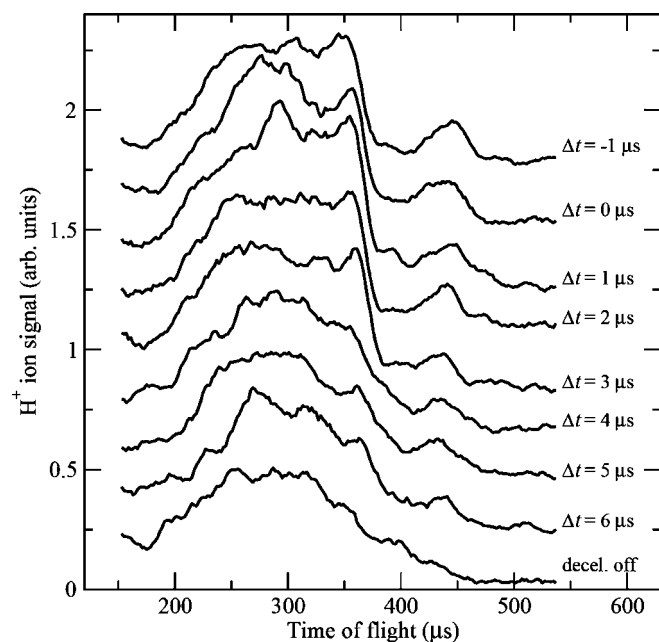


FIG. 8. TOF profiles recorded for a pulse sequence calculated for a synchronous atom with an initial longitudinal velocity of 506 m/s traversing the decelerator at a phase angle of 55° as a function of the delay time Δt between the switch-off and switch-on of adjacent solenoids. The decelerator was operated at a current of 250 A in each case. The bottom profile is the TOF of the H atoms to the detection point when the decelerator is off. For clarity of presentation the upper profiles are vertically offset.

tion are presented in Fig. 8. This figure shows the TOF profiles recorded with a pulse sequence calculated for a synchronous atom with an initial longitudinal velocity of 506 m/s, a phase angle of 55° , and a current of 250 A. The time delay Δt between the switch-off and switch-on of adjacent solenoids was varied from $\Delta t = -1 \mu\text{s}$ in the top profile to $\Delta t = 6 \mu\text{s}$ (second profile from bottom).

The dependence of the TOF profiles on Δt is most apparent when looking at the decelerated and transversely guided features characteristic of the deceleration process, which appear at times of flight of ~ 440 and $\sim 350 \mu\text{s}$, respectively. The late peak corresponding to the phase-stable, decelerated H atom bunches and the sharp edge associated with transverse guiding of the beam of H atoms hardly change in the upper five profiles for which Δt ranges from -1 to $3 \mu\text{s}$. For larger values of Δt , both features gradually disappear until the TOF profile begins to resemble that recorded with the decelerator off. These two observations can be interpreted in terms of a redistribution of the population among the M_F sublevels of the $F=1$ hyperfine state. This redistribution becomes significant for $\Delta t > 3 \mu\text{s}$, i.e., as soon as the time separation between subsequent current pulses becomes longer than the fall time of the pulses. We therefore observe M_F -changing transitions each time a solenoid is switched off if we do not switch on the next solenoid in the sequence sufficiently early.

In order to estimate the probability of M_F -changing transitions which would result in the effects observed experimentally, several particle trajectory simulations have been per-

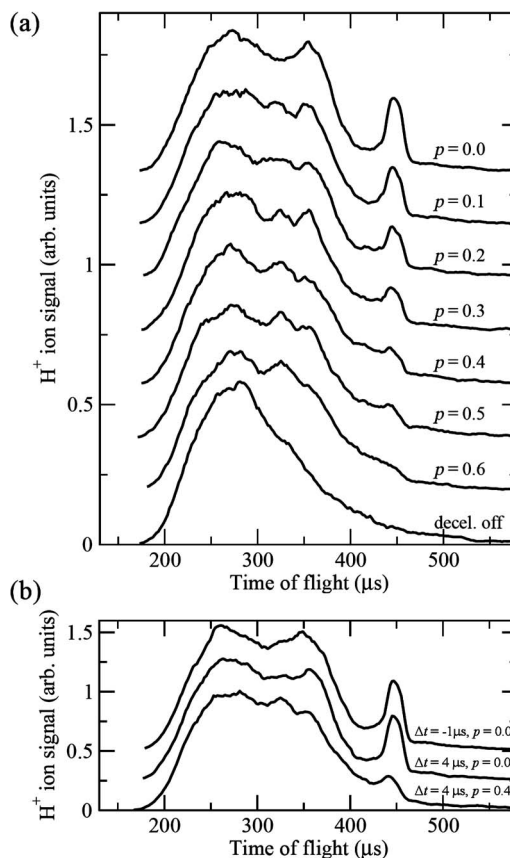


FIG. 9. Simulated TOF profiles for pulse sequences calculated for a synchronous atom with an initial longitudinal velocity of 506 m/s traversing the decelerator at a phase angle of 55° . (a) The probability p of an M_F -changing transition occurring at the switch-off of each of the solenoids increases in increments of 0.1 for each of the profiles moving down the figure. The decelerator was considered to operate at a current of 250 A throughout. The bottom profile is the simulated TOF of the H atoms to the detection point when the decelerator was off. (b) Comparison between simulated TOF profiles calculated assuming that $p=0$ and using pulse sequences for which $\Delta t = -1 \mu\text{s}$ (upper trace) and $\Delta t = 4 \mu\text{s}$ (middle trace), and for which $\Delta t = 4 \mu\text{s}$ with $p=0.4$ (bottom trace). For clarity of presentation the upper profiles in each figure are vertically offset.

formed, each with the same pulse sequence, but assuming different probabilities p for the transitions to different M_F sublevels of the $F=1$ manifold (a definition of p was provided in Sec. III). The TOF profiles which resulted from this set of simulations are presented in Fig. 9(a). Because the M_F changes which occur when the last solenoid is switched off do not affect the measured TOF profiles, only six switch-off processes are relevant in these simulations. Each time one of these six solenoids is switched off, a probability $p/2$ is assumed for a transition to take place to each of the other two M_F states of the $F=1$ manifold. For example, the second TOF profile from the top in Fig. 9(a) is simulated assuming a probability of $p=0.1$ for a M_F change to occur at the switch-off of each relevant solenoid. For an atom in the $M_F = +1$ state, transitions to $M_F = 0$ and $M_F = -1$ are both assumed to take place with a probability of 0.05. As the probability of

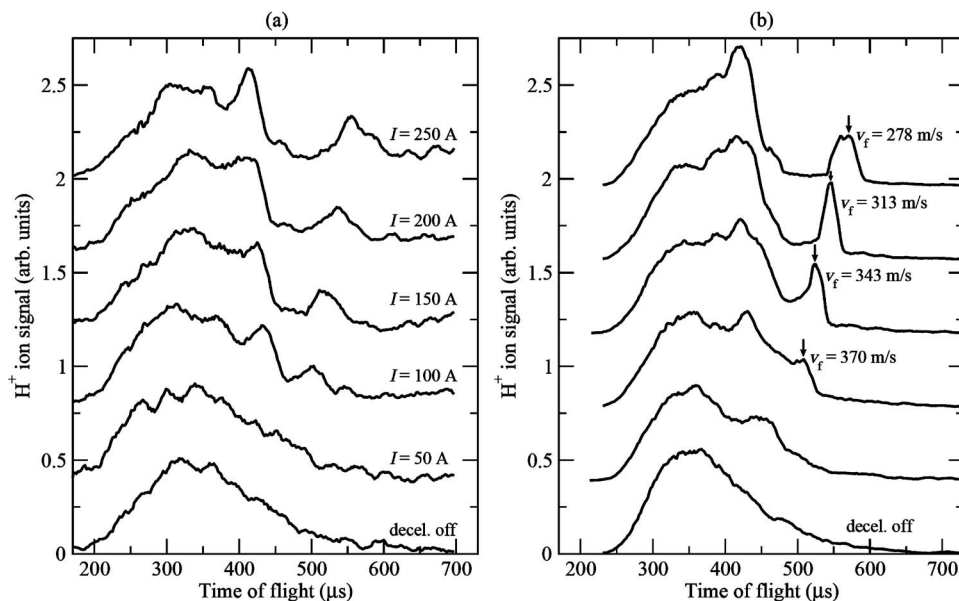


FIG. 10. TOF profiles demonstrating the deceleration of H atoms seeded in Kr for which the synchronous atom has an initial longitudinal velocity of 422 m/s and traverses the decelerator at a phase angle of 55° . The current at which the decelerator was operated was varied from 50 to 250 A (i.e., the maximum magnetic field strength on axis in each solenoid was varied from 0.3 to 1.4 T). The left panel (a) contains the experimental data with the simulated data presented in the right panel (b). The simulated final velocities of the atoms are indicated by the vertical arrows in panel (b). The bottom profile in each panel represents the TOF of the H atoms when the decelerator was off. For clarity of presentation the upper profiles in each panel are vertically offset.

transitions increases, the simulations reveal the progressive weakening and broadening of the peak corresponding to the decelerated bunch of atoms and the gradual disappearance of the peak corresponding to the transversely guided atoms at a TOF of $\sim 350 \mu\text{s}$. This behavior is qualitatively the same as that observed experimentally. Comparing this set of simulations with the experimental data presented in Fig. 8 leads to the conclusion that the changes observed in the experiment at delay times between $\Delta t = 3$ and $4 \mu\text{s}$ correspond approximately to transition probabilities p between 0.3 and 0.4 of an M_F -changing transition occurring at the switch-off of each of the relevant solenoids.

To verify that increasing Δt does not affect the phase stability of the deceleration process, simulations were carried out in which the probability of M_F -changing transitions was assumed to be zero. In Fig. 9(b) the results of two such simulations, carried out for $\Delta t = -1 \mu\text{s}$ (top profile) and $\Delta t = 4 \mu\text{s}$ (middle profile), are compared. The fact that these profiles are almost identical clearly shows that the gradual broadening and disappearance of the decelerated peak in the experimental results presented in Fig. 7 do not originate from a loss of phase stability caused by the increase of Δt , but from M_F -changing transitions. For further comparison, the simulated TOF profile for which $\Delta t = 4 \mu\text{s}$ and $p = 0.4$ is included as the bottom profile in Fig. 9(b). In the simulations for which $p = 0$, the almost complete independence of the results on Δt can be attributed to the facts that (i) the switch-off times in the deceleration pulse sequences are not adjusted when varying Δt , only the relevant switch-on times and (ii) the contribution of solenoid $n+1$ to the magnetic field gradient at the position of the synchronous atom when solenoid n is switched off is very small even though the magnitude of

the field is sufficient to inhibit M_F -changing processes.

This study of the effect of M_F changing on the phase stability of the deceleration process in a multistage Zeeman decelerator demonstrates that it is extremely important to maintain a nonzero magnetic field throughout the deceleration process so as to prevent randomization of M_F , and in turn maximize the deceleration efficiency and obtain the minimum longitudinal temperature of the bunch of decelerated atoms. A simple method to achieve this is to impose a temporal overlap of the current pulses applied to adjacent solenoids throughout the deceleration process.

C. Deceleration of H atoms seeded in a Kr beam

In order to study the deceleration of H atoms initially moving at slower velocities, experiments were also carried out using Kr rather than Ar as the carrier gas. In Fig. 10 a comparison is presented between the TOF profiles obtained using a 10:1 mixture of Kr and NH_3 by operating the Zeeman decelerator at currents between zero (bottom profile) and 250 A top profile and a phase angle of 55° . The pulse sequences were calculated in each case for a synchronous atom moving with an initial longitudinal velocity of 422 m/s, on the slow side of the mean velocity (630 m/s) of the H atoms in the beam. When compared to the deceleration measurements carried out using Ar as the carrier gas (see Fig. 7), these measurements reveal the same overall characteristics, i.e., a late peak corresponding to the decelerated bunch of atoms and the early maximum associated with the transversely guided atoms which enter the decelerator at a phase angle greater than 55° . However, differences are also apparent. First, the decelerated bunch of atoms arrives at

later times than in the measurements carried out with Ar as carrier gas; for example, at the maximal current of 250 A the bunch of decelerated atoms reaches the detection point after $\sim 550 \mu\text{s}$ rather than $\sim 450 \mu\text{s}$ in Fig. 7. Second, the signal-to-noise ratio of the TOF profile obtained when Kr is used as the carrier gas is poorer. We attribute this effect to an increase of the radial velocity components of the H atoms in the gas beam that results from the larger ratio of masses between the carrier gas and the seed gas.

The results of the particle trajectory simulations corresponding to the experimental results in Fig. 10(a) are presented in Fig. 10(b). From these simulations of the times of flight of the decelerated atoms, for the cases when the decelerator was operated at 100, 150, 200, and 250 A, we have extracted values for the final velocities of the decelerated atoms of 370, 343, 313, and 278 m/s, respectively. Thus the total longitudinal kinetic energy removed in each case amounts to 0.21 meV ($\equiv 1.7 \text{ cm}^{-1}$), 0.32 meV ($\equiv 2.5 \text{ cm}^{-1}$), 0.42 meV ($\equiv 3.4 \text{ cm}^{-1}$), and 0.53 meV ($\equiv 4.2 \text{ cm}^{-1}$). These changes in kinetic energy are again in good agreement with those observed in the data presented in Figs. 5 and 7 and exhibit the expected linear variation as a function of the operating current. The agreement between simulated and measured TOF profiles, though satisfactory, is not as good as for the experiments carried out with Ar as the carrier gas (see Fig. 7), primarily because the expansion of the beam of H atoms seeded in Kr was not characterized as extensively as that seeded in Ar.

D. Deceleration of D atoms seeded in a Kr beam

To further study the effect of the mass ratio between the carrier gas and the seed gas on the throughput of the decelerator and to test the reliability of the particle trajectory simulations on a heavier atom, D atoms seeded in Kr have also been decelerated. The undecelerated beam of D atoms was found to have a mean longitudinal velocity of 550 m/s. However, for the sake of comparison with the deceleration behavior of H atoms seeded in Kr, the magnetic field pulse sequence was also calculated for a synchronous atom with an initial longitudinal velocity of 422 m/s, a phase angle of 55° , and a maximal current of 250 A. Under these conditions, the TOF profile of the D atoms displayed in Fig. 11(b) was recorded. These data can be directly compared with the TOF profiles of the H atoms obtained under similar conditions [shown in Fig. 11(a)]. In each case the TOF profiles recorded with the decelerator off are indicated by the dashed curves. The features associated with the transversely guided atoms are located at similar positions in the TOF profiles of H and D. As expected, the late peak indicative of the phase-stable deceleration process is observed at a lower final longitudinal velocity for the H atoms than for the D atoms. The differences between the initial and final kinetic energies extracted from particle trajectory simulations are 0.53 meV ($\equiv 4.2 \text{ cm}^{-1}$) and 0.45 meV ($\equiv 3.7 \text{ cm}^{-1}$), respectively, over the seven deceleration stages. The slight discrepancy in these energy measurements is likely to be related to the accuracy of the input parameters used in the simulations. The differences in the shapes of the TOF profiles recorded with the

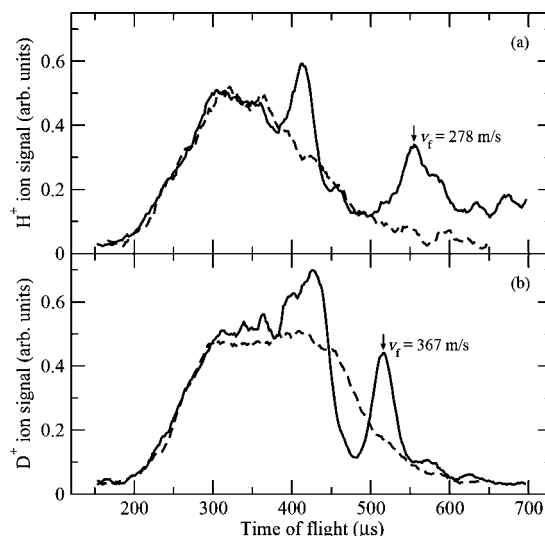


FIG. 11. TOF profiles for (a) H atoms and (b) D atoms seeded in Kr. In both cases the solid curves indicate the measured TOF profiles for pulse sequences calculated for the deceleration of a synchronous atom with an initial longitudinal velocity of 422 m/s that traversed the decelerator at a phase angle of 55° . The decelerator was operated at a current of 250 A in each case (i.e., the maximum magnetic field strength on axis in each solenoid was 1.4 T). The dashed curves indicate the measured TOF profiles at the detection point when the decelerator was off.

decelerator off may be attributed to the difference in transverse velocities of the H and D atoms. Although we cannot directly compare the absolute number of H^+ ions measured to the number of D^+ ions measured, the higher signal-to-noise ratio obtained in the D TOF profile suggests that the throughput of the decelerator is greater for the D atoms than for the H atoms, in accordance with the more favorable mass ratio between the carrier gas and seed gas.

V. CONCLUSIONS

The phase-stable deceleration of H and D atoms produced in seeded supersonic expansions has been demonstrated using a seven-stage Zeeman decelerator. From the analysis of the experiments using particle trajectory simulations we have determined that typically 0.079 meV ($\equiv 0.63 \text{ cm}^{-1}$) of kinetic energy can be removed per stage when currents of 250 A are pulsed through each solenoid and the decelerator is operated under conditions for which phase stability is maintained, with the synchronous atom traversing the decelerator at a phase angle of 55° . Operating each solenoid at this current results in a maximum magnetic field strength on axis of 1.4 T.

The first direct measurements of the effect of M_F -changing transitions occurring at near-zero magnetic field strength on the deceleration process have been made and indicate that the problems associated with such transitions can be avoided provided a nonzero magnetic field is maintained on axis throughout the deceleration process. Particle trajectory simulations reveal that it is important to accurately characterize the transverse spatial and velocity dis-

tributions of the atoms entering the decelerator.

Finally, the demonstration of Zeeman deceleration of H and D atoms produced in supersonic expansions highlights the feasibility of this technique to produce quantum-state-selective cold radicals which may be used in precision spectroscopy and to study reactive collisions and molecular scattering.

ACKNOWLEDGMENTS

We thank B. H. Meier and U. Meier (ETH Zürich) for useful discussions. This work was supported financially by ETH Zürich and the Swiss National Science Foundation under Project 200021-113886.

-
- [1] M. R. Tarbutt, H. L. Bethlem, J. J. Hudson, V. L. Ryabov, V. A. Ryzhov, B. E. Sauer, G. Meijer, and E. A. Hinds, *Phys. Rev. Lett.* **92**, 173002 (2004).
 - [2] P. F. Weck and N. Balakrishnan, *Int. Rev. Phys. Chem.* **25**, 283 (2006).
 - [3] H. L. Bethlem, G. Berden, and G. Meijer, *Phys. Rev. Lett.* **83**, 1558 (1999).
 - [4] H. L. Bethlem and G. Meijer, *Int. Rev. Phys. Chem.* **22**, 73 (2003).
 - [5] S. R. Procter, Y. Yamakita, F. Merkt, and T. P. Softley, *Chem. Phys. Lett.* **374**, 667 (2003).
 - [6] E. Vliegen and F. Merkt, *J. Phys. B* **38**, 1623 (2005).
 - [7] E. Vliegen and F. Merkt, *J. Phys. B* **39**, L241 (2006).
 - [8] N. Vanhaecke, U. Meier, M. Andrist, B. H. Meier, and F. Merkt, *Phys. Rev. A* **75**, 031402(R) (2007).
 - [9] I. R. Sims and I. W. M. Smith, *Annu. Rev. Phys. Chem.* **46**, 109 (1995).
 - [10] O. Stern, *Z. Phys.* **7**, 249 (1921).
 - [11] W. Gerlach and O. Stern, *Z. Phys.* **9**, 349 (1922).
 - [12] W. Gerlach and O. Stern, *Z. Phys.* **9**, 353 (1922).
 - [13] I. I. Rabi, J. R. Zacharias, S. Millman, and P. Kusch, *Phys. Rev.* **53**, 318 (1938).
 - [14] N. I. Wakayama, *IEEE Trans. Magn.* **31**, 897 (1995).
 - [15] E. M. McMillan, *Phys. Rev.* **68**, 143 (1945).
 - [16] V. Veksler, *J. Phys. (USSR)* **9**, 153 (1945).
 - [17] E. Narevicius, C. G. Parthey, A. Libson, M. F. Riedel, U. Even, and M. G. Raizen, *New J. Phys.* **9**, 96 (2007).
 - [18] S. Willitsch, J. M. Dyke, and F. Merkt, *Helv. Chim. Acta* **86**, 1152 (2003).
 - [19] S. Y. T. van de Meerakker, N. Vanhaecke, H. L. Bethlem, and G. Meijer, *Phys. Rev. A* **71**, 053409 (2005).
 - [20] B. Friedrich, *Eur. Phys. J. D* **31**, 313 (2004).
 - [21] T. Bergeman, G. Erez, and H. J. Metcalf, *Phys. Rev. A* **35**, 1535 (1987).
 - [22] E. Vliegen, S. D. Hogan, H. Schmutz, and F. Merkt, *Phys. Rev. A* **76**, 023405 (2007).
 - [23] E. Majorana, *Nuovo Cimento* **9**, 43 (1932).